Structural and spectroscopic characteristics of ZnO and ZnO:Er^{3+} nanostructures

2004 J. Phys.: Condens. Matter 16 7123

(http://iopscience.iop.org/0953-8984/16/39/043)

INSTITUTE OF PHYSICS PUBLISHING JOURNAL OF PHYSICS: CONDENSED MATTER

J. Phys.: Condens. Matter **16** (2004) 7123–7129 PII: S0953-8984(04)75789-6

Structural and spectroscopic characteristics of ZnO and ZnO:Er^{3+} nanostructures

A K Pradhan[1,3], Kai Zhang[1], G B Loutts[1], U N Roy[2], Y Cui[2] and A Burger[2]

[1] Center for Materials Research, Norfolk State University, 700 Park Avenue, Norfolk, VA 23504, USA
[2] Department of Physics, Fisk University, 1000, 17 Avenue North, Nashville, TN 37208, USA

E-mail: apradhan@nsu.edu

Received 28 January 2004
Published 17 September 2004
Online at stacks.iop.org/JPhysCM/16/7123
doi:10.1088/0953-8984/16/39/043

Abstract

We report on the synthesis and characterization of ZnO and Er-doped ZnO nanostructures. ZnO powders were synthesized by the coprecipitation and the combustion techniques. ZnO powders prepared by the coprecipitation method exhibit sheet-like nanostructures. The sheet thickness is found to be less than 100 nm. The structural and spectroscopic properties of ZnO powders and sheet-like nanostructures have been investigated and discussed. The x-ray and Raman studies show the effects of Zn deficiency on sintering the ZnO samples at about 1300 °C in air. The luminescent properties of ZnO:Er^{3+} nanostructures have been illustrated through emission and Raman spectroscopy.

Zinc Oxide (ZnO) is a II–VI compound wide-band-gap semiconductor with a direct band gap of 3.37 eV and a large excitonic binding energy of about 60 MeV at room temperature. ZnO has attracted a great deal of research interest owing to its promising applications in blue light-emitting diodes, field-effect transistors, ultraviolet laser diodes, solar cells, sensors, acousto-electrical devices and detectors. The ZnO nanostructures, such as nanobelt and nanolasers [1, 2], have spurred an intensive research interest in studies on the ZnO nanostructure synthesis and their applications. The recent demonstrations of ZnO nanorods [3], nanowires [4] and nanotubes [5] are very exciting. In addition, the luminescent properties of the doped ZnO are very sensitive to its surface states [6]. The ZnO nano- and microstructures with a high surface-to-bulk ratio are expected to make possible applications in luminescent technology due to their chemical and environmental stability.

Most of the ZnO nanostructures are processed through the thin film technique and are associated with complicated methodology. In this paper, we report a simple wet chemical route, such as coprecipitation, and combustion to synthesize ZnO and Er-doped ZnO nanostructures, and their structural and spectroscopic characterizations. We have demonstrated that ZnO

[3] Author to whom all correspondence should be addressed.

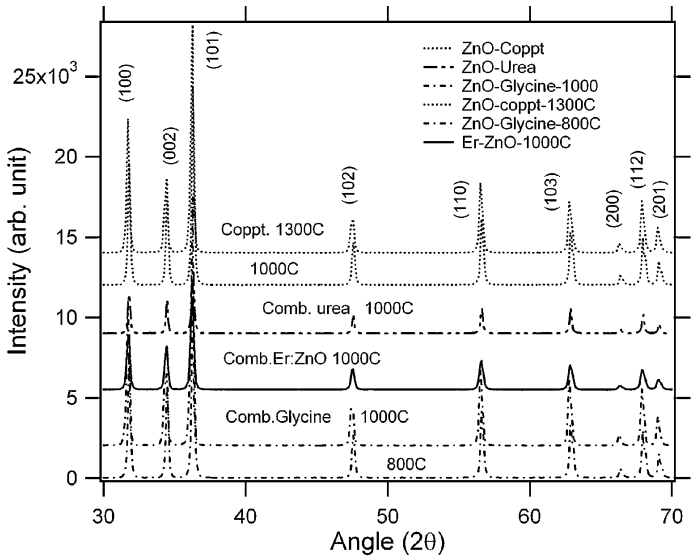

Figure 1. X-ray powder-diffraction (XRD) patterns of ZnO and ZnO:Er^{3+} powders calcined at different temperatures and synthesized through different chemical routes as indicated in the figure.

synthesized by the coprecipitation technique exhibits a sheet-like nanostructure having thickness less than 100 nm. The structural and spectroscopic properties of ZnO powders have been discussed. We have explicitly shown the effects of Zn deficiency through x-ray and Raman studies. In addition, we revealed the effects of Er doping on the luminescent properties of ZnO nanopraticles through emission and Raman spectroscopy.

Phase identification was performed by the x-ray powder diffraction (XRD) method on a Rigaku x-ray diffractometer (XRD) using Cu K_α radiation. The crystallite size of the powder was calculated from the line broadening. Powder and sintered ceramic surface morphology and microstructures were observed by scanning electron microscopy (SEM). The Raman spectra were recorded using a LabRam microRaman spectrometer with He–Ne laser excitation (wavelength: 632.8 nm).

The nanocrystalline ZnO and ZnO:Er^{3+} powders were synthesized using both modified combustion and coprecipitation techniques [7–9] from their respective nitrate solutions. The Er-doping was kept as low as 0.05 at% for all the samples. For the combustion technique, the precursor mixture with urea (1 : 3 = ZnO : urea or glycine) was dehydrated completely before the combustion at a temperature of 600 °C, at which the precursor powders comprising of nanoparticles were obtained. For the coprecipitation method, the well-stirred nitrate solution was mixed with an aqueous solution of NH_4HCO_3 dropwise to form the precipitate. The precipitate slurry was aged for two days at room temperature with continuous stirring, and then filtered and washed with water several times in order to completely remove NH_4HCO_3. Finally, the slurry was washed with methanol ultrasonically followed by final drying at about 100–120 °C. Then the powders were calcined in the temperature region 800–1300 °C for 2–5 h in order to vary the particle size. It is noted that the precursor powders prepared by both the techniques were very loosely agglomerated and can be pulverized very easily.

Figure 1 shows XRD patterns of the ZnO and Er-doped ZnO powders synthesized by several techniques and with different calcination temperatures. The diffraction peaks for all XRD patterns can be indexed to a hexagonal wurzite structured ZnO. The Er-doped sample

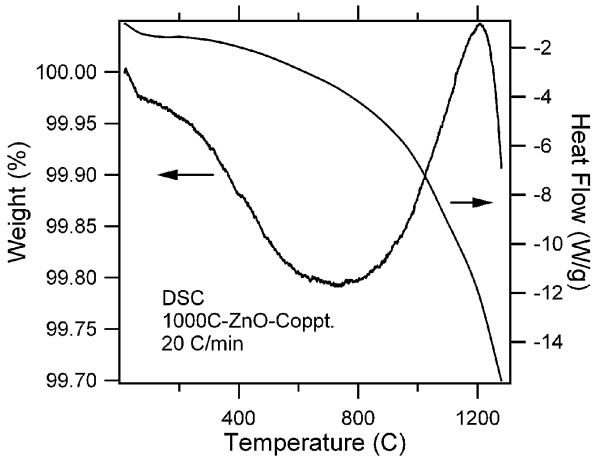

Figure 2. Differential scanning calorimetry and heat flow of ZnO powders (coprecipitation route) calcined at 1000 °C.

did not show an additional peak in the XRD pattern as reported [10] for the bulk target having 0.5 wt% of Er_2O_3 in ZnO. The particle size calculated from the x-ray line broadening for the combustion-synthesized powders is less than half of the size of the powders (∼90 nm) prepared by the coprecipitation technique. The smallest particle size of 35 nm was found for the powders synthesized by the combustion technique using glycine. It is noted that the particle size does not increase significantly on increasing the sintering temperature from 1000 to 1300 °C for the samples prepared by the coprecipitation route. However, all intensity peak positions shifted to lower angles for the sintered sample at 1300 °C in air, indicating a slight change in lattice constants. In order to explore more about the change in the peak positions, we show the differential scanning calorimetric (DSC) results in figure 2 for this sample. A distinct peak, although very small, is seen in the weight loss above 1200 °C, suggesting probably a loss of a very small amount of Zn from the surface through the sublimation process. Hence, it is necessary to sinter ZnO in oxygen overpressure, once the sintering temperature is above 1200 °C.

Figure 3 shows the SEM images of ZnO powders synthesized by the above-mentioned techniques. Figures 3(a)–(c) are the SEM micrographs for the powders synthesized by combustion (using urea), combustion (using glycine) and coprecipitation techniques with a subsequent calcination temperature of 1000 °C for 2 h. It is very clear that the particle sizes are the smallest for the powders synthesized by the combustion techniques using glycine. However, it is remarkable to note that the powders synthesized by the coprecipitation route show nanostructures (figure 3(c)), comprising of 1–2 μm length and sheet width of less than 100 nm, stacked on each other. These structures also clearly show the hexagonal symmetry, and sometimes each sheet is joined together to form a larger plate. Figure 3(d) shows the sheet-like microstructure in an enlarged form. This suggests that a simple chemical route can produce nanostructures of ZnO, although detailed high-resolution SEM and transmission studies are necessary to visualize the nanostructural morphology more clearly. Similar features were also observed for Er-doped ZnO.

Figure 4(a) shows the porous nanostructure of ZnO powders synthesized by the combustion technique using glycine, followed by calcination at 800 °C. The porous structures transform into an aggregate of large particles after sintering at 1300 °C for 2 h as shown in figure 4(b).

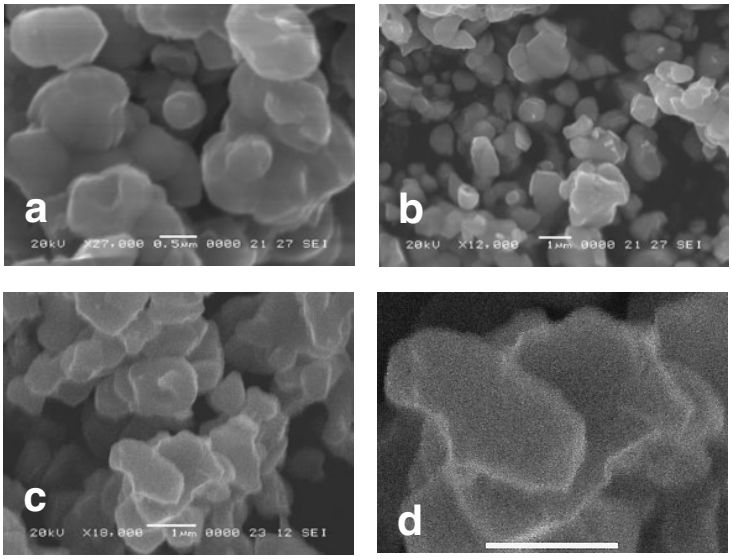

Figure 3. Scanning electron micrographs of ZnO powders calcined at 1000 °C, (a) combustion (urea), (b) combustion (glycine), (c) coprecipitation and (d) coprecipitation (enlarged scale, the bar represents 1 μm).

However, similar sintering for the powders synthesized by the coprecipitation route yields grains having hexagonal symmetry and the grains are fused forming a neck. We speculate that a very low amount of Zn may escape from the surface of the grain through a sublimation process at 1300 °C when sintered in air, and it may be the predominant reason for a slight shift of XRD lines towards the lower angle side, indicating the onset of a structural change. However, detailed compositional analysis is necessary to confirm this change.

The wurzite structure of ZnO belongs to the space group $C_{6v}{}^4$ with two formula units per primitive cell where all the atoms occupy C_{3v}. Eight sets of zone centre optical phonons, $2A_1 + 2E_2 + 2E_1 + 2B_1$, are predicted according to the group theory analysis. The A_1 and E_1 modes are polar and split into transverse-optical (TO) and longitudinal-optical (LO) phonons, and the E_2 mode consists of two modes of low- and high-frequency phonons. On the other hand, the B_1 modes are not Raman-active. Figure 5 shows the Raman spectra of ZnO nanosheet-like structures from two different techniques and a sample with a partially Zn-deficient surface by high-temperature annealing. The most intense peak at 437 cm^{-1} corresponds to the vibrational mode of $E_2{}^{high}$, and it is a typical Raman peak of ZnO bulk. The additional low intensity peaks observed in figure 5 are assigned to their respective modes. The modes at 203, 333 and 664 cm^{-1} are due to the multi-phonon scattering process [11]. On the other hand, the E_1 (LO) mode 581 cm^{-1} is caused by the defect due to O-vacancy, Zn-interstitial defect states, or these complexes and free carriers. It is interesting to note that the E_1 (LO) phonon mode in high-temperature-annealed sample has undergone broadening of the line width, frequency down shift and asymmetric line shape (shown as asterisks in figure 5). Although this may be due to strong coupling of free carriers with E_1 (LO) mode, the influence of change in particle size due to high temperature annealing cannot be ruled out.

In figures 6(a) and (b), we have shown the emission and Raman spectra of Er^{3+}-doped ZnO nanostructures, mainly prepared through a coprecipitation technique, to demonstrate their luminescent behaviour and Er^{3+}-doped Raman spectra. The emission spectra, shown in figure 6(a), were recorded in the wavelength range 600–1000 nm under three different

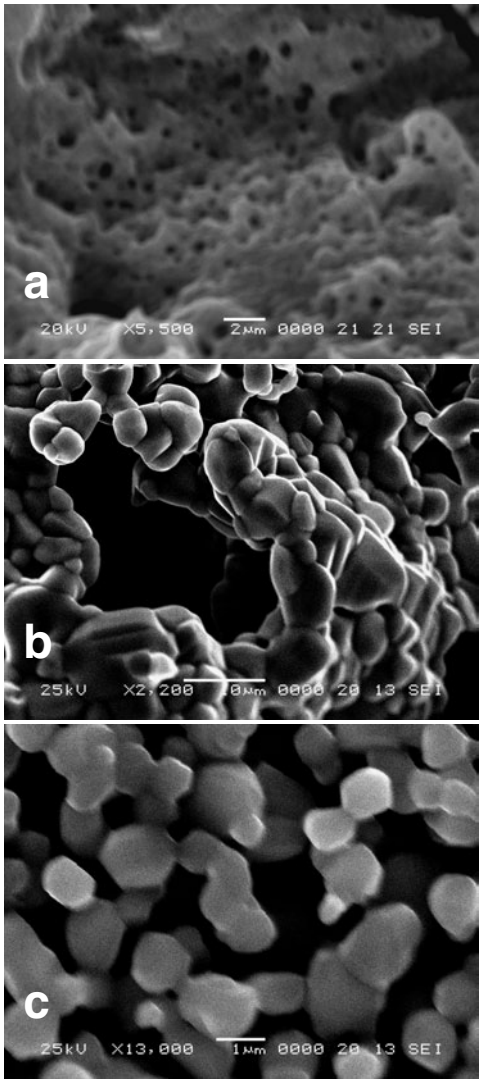

Figure 4. Scanning electron micrographs of ZnO powders, (a) combustion (glycine, calcined at 800 °C), (b) combustion (glycine, calcined at 1300 °C), and (c) coprecipitation (calcined at 1300 °C).

excitation conditions. The spectra exhibit several interesting features. The broad background found in all samples over the whole region of the emission spectra may be considered due to deep trapping centres within the bang-gap of the ZnO host. Under all three excitations, an intense peak at 998 nm, corresponding to $^4I_{11/2} \rightarrow {}^4I_{15/2}$ was observed. The excitation at 490 nm yields the transition at 665 nm, which corresponds to $^4F_{9/2} \rightarrow {}^4I_{15/2}$, and the excitation at 526 nm exhibits transition at 864 nm that corresponds to $^4S_{3/2} \rightarrow {}^4I_{13/2}$. The peak at 864 nm is caused by the optical transition between the 5th excited state $^4S_{3/2}$ and the 1st state $^4I_{13/2}$ and is believed to relax from the direct absorption level and will generate the 1.54 μm luminescence (not shown here). In contrast, the emission spectra under different excitations other than 526 nm reveal the $^4S_{3/2} \rightarrow {}^4I_{13/2}$ transition. On the other hand, several transitions were observed in the vicinity of

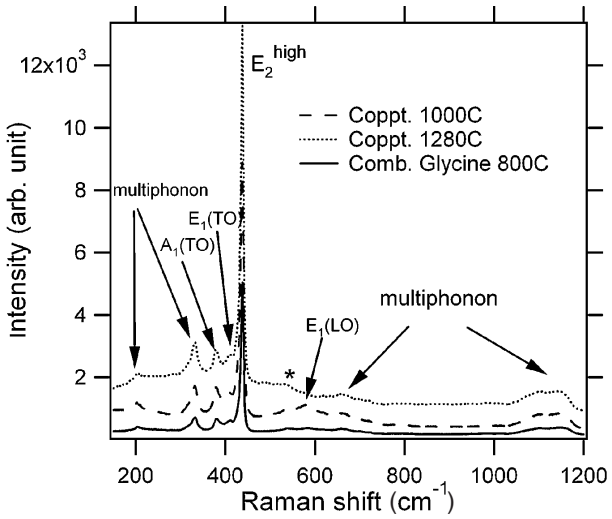

Figure 5. Raman shifts of ZnO powders synthesized by coprecipitation technique and calcined at 1000 and 1280 °C. Raman shifts of ZnO nanopowders prepared by the combustion method using glycine are also shown.

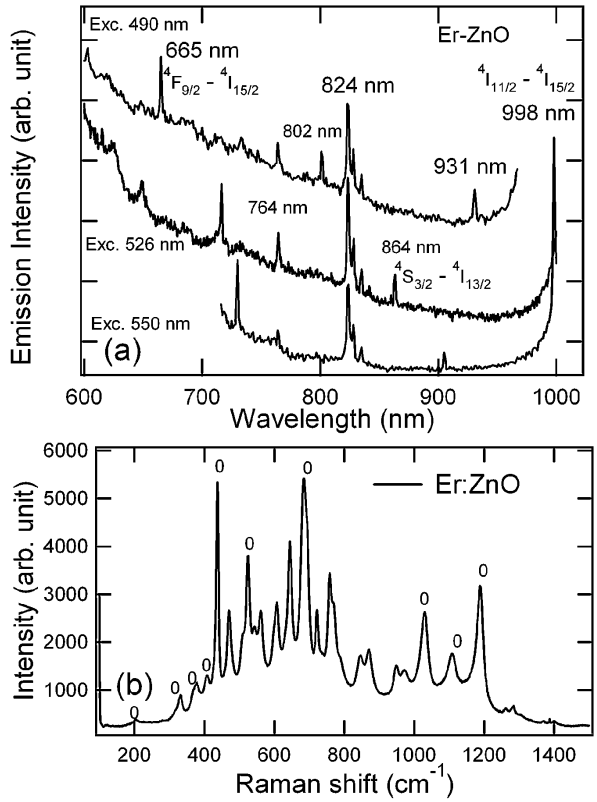

Figure 6. (a) Emission spectra of Er-doped ZnO powders prepared by coprecipitation method shown for three different excitations. (b) Raman shift of Er-doped ZnO powders.

825 and 764 nm for all present excitations. These features were absent in Er-doped thin films [10, 12], probably due to poor intensity of these lines in films.

The Raman spectra of Er-doped ZnO, shown in figure 6(b) show all vibrational modes (marked) seen in ZnO bulk samples as described earlier. Several interesting features were observed on doping Er into ZnO. The E_1 (LO) mode at 581 cm^{-1} caused by the defect due to O-vacancy has a sharp feature with enhanced intensity. In addition, the Raman-active modes above 600 cm^{-1} have well-developed features, suggesting stronger multiphonon scattering contributions. The additional Raman lines observed in the spectra are due to Er_2O_3 activation in the ZnO host.

In conclusion, we have demonstrated that the ZnO and Er-doped ZnO nanostructures can be synthesized through a simple wet chemical route. We have shown that ZnO synthesized by the coprecipitation technique exhibits a sheet-like nanostructure having a thickness less than 100 nm. The structural and spectroscopic properties of ZnO powders have been investigated and discussed. The x-ray and Raman studies show the effects Zn deficiency on sintering the ZnO samples at about 1300 °C in air. In addition, we revealed the luminescent properties of ZnO:Er^{3+} nanostructures through emission and Raman spectroscopy. Er introduces additional defects that cause many intense Raman lines due to enhanced multiphonon vibrations.

Acknowledgment

This work is supported by the NASA URC cooperative agreement NCC-3-1035 and NSF CREST grant HRD-9805059.

References

[1] Pan Z, Dai Z R and Wang Z L 1998 *Science* **281** 973
[2] Huang M *et al* 2001 *Science* **292** 1897
[3] Wu J-J, Liu S-C, Wu C-T, Chen K and Chen L-C 2002 *Appl. Phys. Lett.* **81** 1312
[4] Huang M H, Wu Y, Feick H, Trans N, Weber E and Yang P 2001 *Adv. Mater.* **13** 113
[5] Park W I, Kim D H, Jung S W and Yi G-C 2002 *Appl. Phys. Lett.* **80** 4232
[6] Yao B D, Shi H Z, Bai H J and Zhang L D 2000 *J. Phys.: Condens. Matter* **12** 6265
[7] Shikao S and Jiye W 2001 *J. Alloys Compounds* **327** 82
[8] Ikesue A, Furosato I and Kamata K 1995 *J. Am. Ceram. Soc.* **78** 225
[9] Saito N, Matsuda S and Ikegami T 1998 *J. Am. Ceram. Soc.* **81** 2023
[10] Komuro S, Katsumata T, Morikawa T, Zhao X, Isshiki H and Aoyagi Y 2000 *Appl. Phys. Lett.* **76** 3935
[11] Cheng B, Xiao Y, Wu G and Zhang L 2004 *Appl. Phys. Lett.* **84** 416
[12] Zhao X, Komuro S, Isshiki H, Aoyagi Y and Sugano T 2000 *J. Lumin.* **87–88** 1254